Journal of Power Sources 195 (2010) 5235–5245

Contents lists available at ScienceDirect

Journal of Power Sources

journal homepage: www.elsevier.com/locate/jpowsour

On the temperature distribution in polymer electrolyte fuel cells

J.G. Pharoah [a,*], O.S. Burheim [b]

[a] Fuel Cell Research Centre, Queen's University, 945 Princess Street, Kingston, Canada
[b] Norwegian University of Science and Technology (NTNU), 7491 Trondheim, Norway

ARTICLE INFO

Article history:
Received 19 October 2009
Received in revised form 22 January 2010
Accepted 6 March 2010
Available online 12 March 2010

Keywords:
PEM fuel cells
Temperature distribution
Heat sources
Water phase change
Cell design

ABSTRACT

This paper presents 2D thermal model of a fuel cell to elucidate some of the issues and important parameters with respect to temperature distributions in PEM fuel cells. A short review on various properties affecting the temperature profile and the heat production in the polymer electrolyte fuel cell is included. At an average current density of 1 A cm^{-2}, it is found that the maximum temperature of the MEA is elevated by between 4.5 and 15 K compared to the polarisation plate temperature. The smallest deviation corresponds to one dimensional transport, while the largest corresponds to the two dimensional transport considering anisotropic thermal conductivity. The two dimensional thermal model further predicts increased lost work. While most of the heat generation is allocated in the cathode, it is shown that the heat effect may be balanced by the water phase change in the anode. The most significant factor in determining the temperature distribution is the gas channel geometry (width and channel type), followed by the thermal conductivity of the porous transport layer and state of the water in the cell.

1. Introduction

The vast majority of fuel cell work, both experimental and theoretical, assumes isothermal conditions when in reality isothermal conditions are extremely difficult to maintain, especially at moderate and high current densities. Single cells are often externally heated during experiments while stacks require significant cooling and temperature gradients will exist both within a cell and within the stack. Understanding the temperature distribution is important not only as the lost work from reversible heat is temperature dependant, but also because the membrane may be exposed to a detrimental temperature and humidity regime. In addition, elevated temperatures contribute to degradation rates which can be exacerbated by high temperatures and large gradients. Further, the effect of water phase change can, depending on the rate, have a significant impact on the resulting temperature distributions.

The operating temperature of a fuel cell is usually taken to be the temperature measured at some distance from the electrodes, often in the end plate, and this value can be significantly different from temperature at the electrodes. In fact, some measurements have shown that the temperature in the gas channels can be as much as 8 °C cooler than that adjacent to the electrode itself [1]. While the effects are smaller, this trend is also demonstrated in non-optimised cells with unique temperature sensors embedded in the electrolyte [2]. Knowing the actual temperatures at the electrodes is important for several reasons: (a) the reaction kinetics are dependent upon the temperature of the electrode, (b) the transport properties are functions of the local temperature, (c) the rate of phase change is strongly dependent on the local temperature and (d) Nafion electrolytes must be reasonably maintained below 120 °C at 1 atm to avoid irreversible damage by humidified air [3].

According to Bauer et al. [3,4] Nafion will significantly and permanently decrease its ionic conductivity at elevated temperature. The elastic strength of Nafion, the E-modulus, was measured both as a function of temperature and as a function of access to water. This property is lowered by increased temperature and increased water accessibility. When the E-modulus is sufficiently weakened and water is adequately accessible, the membrane material will swell to self-destruction. Nafion is resistant to failure by temperature elevation if the access to water is limited. It was revealed that Nafion exposed to 100% RH at 1 atm will undergo irreversible damages at 120 °C. Between 90 and 95 °C, Bauer et al. found that the E-modulus of Nafion in contact with liquid water started to decrease dramatically with increased temperature. This result suggests that Nafion in contact with liquid water at approximately 95 °C may undergo detrimental changes. Further, it was shown that by lowering the relative humidity the maximum temperature recommendation for Nafion would increase, i.e. at 1 atm approximately 91% RH/130 °C, 85% RH/140 °C and 75% RH/150 °C. Taking

Abbreviations: BPP, bi-polar plate; HP, high compaction pressure; LP, low compaction pressure; MPL, micropouros layer; PEM, polymer electrolyte membrane; PTL, porous transport layer.

* Corresponding author. Tel.: +1 613 533 6579; fax: +1 613 533 6489.
E-mail addresses: pharoah@me.queensu.ca (J.G. Pharoah), burheim@gmail.com (O.S. Burheim).

0378-7753/$ – see front matter © 2010 Elsevier B.V. All rights reserved.
doi:10.1016/j.jpowsour.2010.03.024

Nomenclature

j	current density ($A\,cm^{-2}$)
k	thermal conductivity ($W\,K^{-1}\,m^{-1}$)
E	electrochemical potential (V)
H	enthalpy of reaction ($J\,mol^{-1}$)
I	current (A)
Q'	heat flux ($W\,m^{-2}$)
S	entropy of reaction ($J\,mol^{-1}\,K^{-1}$)
T	temperature (K or °C)
W	width of channel (m)

Greek letters

α	net water drag
ζ	vapour multiplier ($\alpha + 0.5$)
η	combined overpotential (V)
κ	conductivity of membrane ($S\,m^{-1}$)
λ	water content in membrane water/sulphonic group
σ	amplitude of current distribution
Δ	change in state

into account Nafions response to temperature elevation, water accessibility and that water is liquid up to almost 120 °C (for gases at 2 atm), a PEMFC may, in this region (90–120 °C), be irreversibly damaged. It is well known among most fuel cell scientists that Nafion is better humidified by liquid water than from fully humidified air—despite equal chemical potentials of water in the two cases. This is known as Schroeder's Paradox [5]. The weakening of Nafion at some high temperature conditions may lead to cracking of the membrane under fuel cell operation. The temperature range chosen for the measurements [3] may have been based on an understanding that the fuel cell was isothermal, as was the general perception around 2001. Additionally, it should be mentioned that modified Nafion materials, typically containing zirconia, sustain both higher temperatures and gas pressures under operation and that increased temperature improves the kinetics of the fuel cell reaction [6]. Nevertheless, the temperature gradients within the fuel cell are of the same significance regardless of whether the operation temperature in the bi-polar plate is 50, 80 or 120 °C.

The factors which significantly affect the temperature distribution include: (1) component conductivities, (2) contact resistances, (3) heat losses from the system, (4) the electrode reactions, (5) the local rate of water phase change and (6) the geometry of the cell. Point one and two refers to the selected materials for the cell, the compaction forces and the local environment, i.e. residual water. Recently, Burheim et al. [7] demonstrated how the increasing compaction pressure and residual water in the PTL increases the through plane thermal conductivity of PTLs. However, these results consider only the through plane thermal conductivity. According to Ramousse et al. [8], based on the model by Danes and Bardon, the in-plane thermal conductivity of a PTL should be between ten and twenty times the through plane thermal conductivity, depending on the fibre structure. Ironically, Danes and Bardon developed the model for porous carbon fibre felts intended for insulation [9]. However, measurements of in-plane thermal conductivities are not yet reported. Because measurements of through plane thermal conductivity support the modelling work by Ramousse and Bardon, it is very likely that the PTL is highly anisotropic, though the in-plane thermal conductivity may not depend on compaction pressure and residual water to the same degree as the through-plane thermal conductivity. Nitta et al. [10] studied the effect that the flow channel has on the PTL structure. By compressing a Sigracet PTL to different fractions of the original PTL thickness with a surface having a small hole (presenting the gas flow channel) the thickness of PTL material intruding into the gas channel was measured. It was found that compressing a 380 μm PTL to 300 μm under the land resulted in a PTL channel intrusion of approximately 70 μm, meaning that the PTL is almost not compressed under the gas channels for such and smaller compressions.

The lost work in the fuel cell, i.e. ohmic heating and the overpotential, as well as the local rate of water phase change will depend on local temperatures and current density deviations in the fuel cell. Pharoah et al. [11,12] report that, if running a fuel cell at moderate to high current densities, a serpentine gas flow channel will give decreased current underneath the channel while parallel flow fields will have the opposite effect. The prediction is based on modelling a half-cell, using an air cathode. Reum et al. [13] report measurements of similar effects for a fuel cell using parallel gas flow channels. Running their fuel cell at moderate current density of $0.4\,A\,cm^{-2}$ with fully humidified oxygen/hydrogen the maximum current density underneath the gas channel is twice the minimum current density below the lands. Replacing oxygen with air increases this effect so that the maximum current density is more than ten times the smallest.

There is a large body of modelling based work in the literature and only recently has it become common to model thermal affects. This situation is well summarized by Bapat and Thynell [14]. Bapat and Thynell introduce a model similar to this work, neglecting water management, possible current density profiles and different thermal conductivities of both the PTL and its contact to the polarisation plate [14]. Additionally, the basis for several of the heat transport parameters was not up to date or thoroughly based on experimental values. Considering the experimentally *and* theoretically verified effects the gas flow field design imposes to the current density distribution and that the MEA is literally insulated by its surrounding PTL, we present a 2D thermal model of a fuel cell to elucidate some of the issues and important parameters in fuel cell design. The goal of this paper is to present a simple and efficient model to estimate the maximum temperature generated within a fuel cell, and to distinguish those parameters which are most important in determining this maximum.

2. A 2D thermal model

A steady 2D thermal model is developed using the commercial finite element code COMSOL Multiphysics 3.3. A 1D thermal model was also developed, primarily for comparison to other 1D thermal models. This was done simply by replacing the gas channel volume with the polarisation plate material. We give the problem geometry first, the thermodynamics second and the model formulation at the end of this section.

2.1. The problem geometry

The domain of interest is depicted in Fig. 1 and includes bi-polar plates, porous transport layers (sometimes referred to as gas diffusion layers) coated with micro porous layers, catalyst layers and a Nafion electrolyte. All dimensions are given in Fig. 1. The gas flow channel geometry was chosen as a repetitive pattern, 1 mm × 1 mm, except where otherwise noted. Thermal contact resistance is accounted for between the bi-polar plate, and the porous transport layer, but is currently neglected for all other interfaces. This is a reasonable assumption, since the MEA is hot pressed, reducing most other contact resistances in the system. It has been shown for a PTL, very similar to the one investigated by Nitta et al. [10], that the under land compression at 5–15 bar compaction pressure leads to approximately 5–10% compression [7]. Thus it

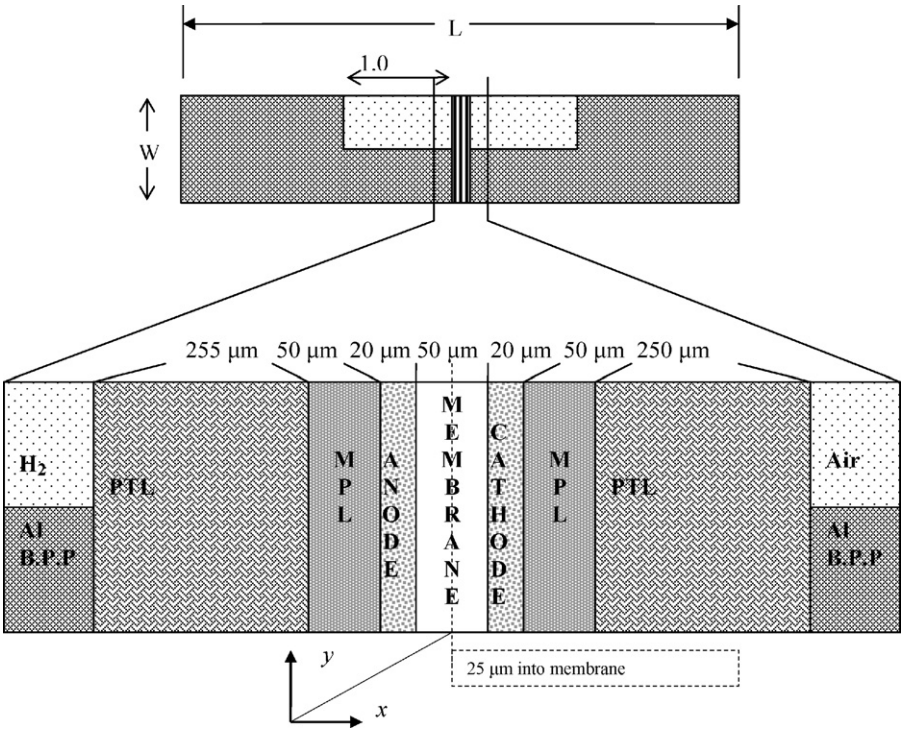

Fig. 1. Problem geometry used for the modelling.

is suggested that the PTL material for all practical reasons would bulge 10–20 μm into the 1 mm deep gas channels, considering the compaction pressures recommended by most PTL manufacturers. Neglecting this bulge is therefore a good simplification when using the model geometry of Fig. 1.

2.2. Thermodynamic background

In order to optimise a fuel cell, it is important to understand where potential work is lost. Eq. (1) follows directly from the first law of thermodynamics written per unit time. The work per unit time extracted from the system is the power delivered by the fuel cell, P_{FC}. Assuming that the reactants enter the system at the same temperature and pressure as the products leave the system, the change in internal energy is given by the change in free energy for the fuel cell reaction, $\Delta G = \Delta H - T\Delta S$. A real system will also lose heat to the environment, due to (i) the energy needed to drive the electrochemical reaction (often referred to as activation losses), ηj, and (ii) due to ohmic heating, Rj^2. This can be expressed as the second half of Eq. (1), where the thermo-neutral voltage, $E_{tn} = -\Delta H/nF$ expresses the total energy, and all other terms represent losses from the point of view of power extracted from the fuel cell. The term related to the entropy change for the reaction, $T\Delta S$, gives rise to a heat release which is reversible, Q_{rev} while the other two terms are irreversible. For the PEM fuel cell reaction the entropy is negative and the reversible heat represent lost work proportional to the temperature. We shall see how this reversible heat production is dependent on the local reaction temperature imposed by cell design and further the available electrochemical potential. We will also evaluate the lost work due to the activation overpotential by considering that it changes with current distributions imposed by gas flow channel design.

$$P_{FC} = -\frac{\Delta H}{nF}j + \frac{T\ \Delta S}{nF}j - \eta j - Rj^2 = E_{TN}j + Q'_{rev} - Q'_{\eta j} - Q'_{\Omega} \qquad (1)$$

2.3. Model formulation

Since the goal of this work is to predict the temperature distribution within a fuel cell, we solve the heat diffusion equation over the domain shown above, and apply source terms to account for the heat generated by each of the mechanisms discussed above. One additional consideration however relates to the phase changes of water within the system. In considering the entropy and enthalpy changes for the fuel cell, a choice has to be made for the state of the product water. If water vapour leaves the system, then the enthalpy change is lower while if it leaves as liquid, it is higher by the heat of vaporisation of water. It is still possible however for water to undergo phase changes within the system which can significantly change the temperature distribution. These changes do not affect overall conservation of energy though, as long as water enters and leaves the system in the same phase and the appropriate enthalpy and entropy changes are used. As an argument to consider the different water scenarios later introduced in the modelling work one can think of different ways to operate fuel cells in practice. Some modern fuel cells are designed to be self humidified under operation, meaning that the feed gases are not required to be humidified. On the other hand, some fuel cells are operated with partially or fully humidified feed gases. As such, the effects imposed by the water management are important to bear in mind when modelling thermal effects in fuel cells. In the present model, water profiles are not explicitly solved for but the temperature effects due to phase change of water are accounted for by assuming a net drag of water, α, condensing (absorbing into the membrane) at the anode and a maximum of this water plus the electrochemically produced water, ζ, progressing to the vapour state by evaporation (desorption) at the cathode. Various assumptions about the state of water can be investigated by independently varying α and ζ. For example, an operating condition with a well-humidified anode but a dryer cathode would correspond to an α close to 1.2, with most of the product water evaporating such that $\zeta = 1.7$. As the cathode humidity increases, both ζ and α will drop. In the case of a dry anode

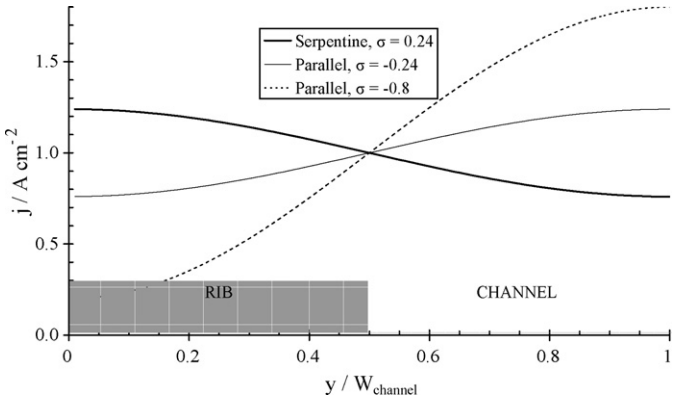

Fig. 2. The current distributions used in the model. The current densities are imposed from applying different gas flow channel patterns and choice of gas on the cathode side.

however, there is no water available in the gas stream such that α would be close to zero. These parameters will be used in order to estimate the relative contribution of phase change on the temperature distribution in the extreme cases. The water content in the membrane is considered to be homogeneously distributed. This may seem as a rough and shallow assumption at first glance because the water is likely not to be evenly distributed. Both the thermal and electric conductivity depend strongly on the local water content. On the other hand, as shall be demonstrated, the ohmic heating imposed by electric current through the membrane is by far the smallest heat source in the system, meaning that the results are not sensitive to this assumption.

The model considers only two dimensions, but different current distributions across the channel (in the y-direction) are imposed by the flow channel design and thus we can compare 3D-like flow channel designs. As discussed above, a serpentine flow field results in a maximum current underneath the land, while a parallel flow field results in a maximum current under the channel [11–13]. Here, we have chosen to impose characteristic distributions using half a period of a cosine function.

$$j(y) = \bar{j}\left(1 + \sigma \cos\left(\frac{\pi}{W}\cdot y\right)\right) \tag{2}$$

where W is the channel dimension and σ is the desired amplitude. Fig. 2 depicts the cross-channel current density distributions used in this model. The amplitude of the distribution is relatively small (except in one case) such that the results should predict the minimum effect of flow field on temperature distribution. The amplitude, σ, in Eq. (2) was chosen such that the temperature along the midline of the membrane was as constant as possible. Again, one exception was made; switching from oxygen to air and broadened flow channels and ribs appear to dramatically increase the amplitude in the current distribution [13]. The three current distributions are sketched in Fig. 2, note that the x-axis in the figure is as the fractional length of the channel width (1 and 2 mm, both typically used in fuel cell setups).

Considering that the compaction pressure is unevenly distributed under the rib and under the channel, the thermal conductivity in the PTL will consequently also vary. In the presented model two extreme distributions were chosen; (a) isotropic and homogeneous thermal conductivity and (b) anisotropic and non-homogeneous thermal conductivity. In the case of an anisotropic PTL, the in-plane conductivity, $k_{=}$, is taken as eight times the lowest measured through plane value, $k_{\perp}$ [8], i.e. $k_{=} = 8{\cdot}k_{\perp}$, dry = 2.16 W K^{-1} m^{-1}. A non-homogeneous distribution of thermal conductivity arises due to the uneven pressure distribution imposed on the PTL by the bi-polar plate. In this case, we have imposed a cosine distribution to account for the variation from under the land (High Pressure) to under the channel (Low Pressure). This distribution is given in Eq. (3).

Table 1
Material thermal properties for the domains depicted in Fig. 1 [7].

	Dry	Wet[a]
Contact resistivity PTL-BPP—$R''_{PTL\text{-}BPP}$ (10^{-4} m^2 K W^{-1})	1.8	0.9
Through plane thermal conductivity PTL—$k_{\perp,LP}$ (4.6 bar)/W K^{-1} m^{-1}	0.27	0.45
Through plane thermal conductivity PTL—$k_{\perp,HP}$ (9.3 bar)/W K^{-1} m^{-1}	0.36	0.54
Thermal conductivity of MPL and catalyst layer k (W K^{-1} m^{-1})	0.5	0.5
Thermal conductivity membrane ($\lambda = 10$) k_{Nafion} (W K^{-1} m^{-1})	0.21	0.21

[a] PTL with residual water.

Unless otherwise stated, values for the thermal conductivities under various conditions are taken from measurements undertaken in our lab for SolviCore materials and for Nafion under various conditions [7]. Table 1 summarizes values used for the model. It is of note that the thermal conductivity of the PTL increases in the presence of liquid water due to the increased fibre to fibre contact. Accordingly, we give thermal conductivities for the two cases.

$$k_{\perp}(y) = \frac{k_{\perp,HP} + k_{\perp,LP}}{2} + \frac{k_{\perp,HP} - k_{\perp,LP}}{2} \cos\left(\frac{\pi}{\delta_{channel}}\cdot y\right) \tag{3}$$

The boundary conditions used for all simulations are Dirichlet conditions (T = 353.14 K) along the y-axis at the edge of the bi-polar plates ($x = -L/2$ and $x = L/2$) and no flux, or symmetry, along $y = 0$ and $y = W$. The dimensions are as shown in Fig. 1 and the material thermal properties are given in Table 1.

Thermal generation is included for:

1. Reversible heating ($T\Delta S$) in the anode and cathode catalyst layer, using the local temperature and $\Delta S_{Anode} = -0.104$ J mol$^{-1}{}_{water}$ K^{-1} and $\Delta S_{Cat} = 163.18$ J mol$^{-1}{}_{water}$ K^{-1} [15] corresponding to the half-cell reactions at standard conditions.
2. Irreversible heating (ηj) due to lumped fuel cell overpotentials of $\eta_{Anode} = 0.001$ V and $\eta_{Cat} = 0.5 + 0.07\ln[j]$ V. This corresponds to imposing the working voltage of the fuel cell at the chosen current density, given as A cm^{-2}, and is measured with a running fuel cell in our laboratory. The anode overpotential, η_{Anode}, is considered to be independent of the local current density distributions, which is reasonable since this contribution to the heating is vanishingly small.
3. Ohmic heating in the membrane (Rj^2) based on a fixed membrane conductivity of 8.7 S m^{-1} corresponding to ten waters per sulphonic group [16]. For a well-humidified fuel cell, 14–21 waters per sulphonic group are considered realistic. The ohmic heating is reduced by increased water content in the membrane. As shall be demonstrated, ohmic heating of the fuel cell is by far the smallest heat generation within the fuel cell and thus the results will not be overly sensitive to this parameter.
4. Water absorption and desorption in Nafion. When water vapour absorbs in Nafion, a heat source is applied as 44.7 kJ mol^{-1}, and when water desorbs to the vapour phase, a heat sink is applied as −44.7 kJ mol^{-1}. These values have been measured by Reucroft et al. [17] for water contents greater than $\lambda = 5$. According to these measurements, there is no heat sink or source when liquid water enters or leaves the membrane for $\lambda > 5$. This is in agreement with other work showing that there is very little interaction between the membrane material and water except for the first three waters per sulphonic group [18]. The bottom line here is that when water molecules enter and leave the membrane, for

Table 2
Some predicted thermal signatures for a PEMFC imposed by various water phase change conditions in the electrodes. The polarisation plate is considered to be operated at 80 °C.

Set	α (water proton^{-1})	ζ (water proton^{-1})	Flow channel design	Thermal conductivity conditions	Q'_{Anode} (kW m^{-2})	$Q'_{Cathode}$ (kW m^{-2})	$T(25, 0)$ (°C (μm, mm))	$T(25, 1)$ (°C (μm, mm))	T_{max} (°C)
0	1.2	1.7	1D	Wet	3.61	2.66	82.1	82.1	82.3
1	1.2	1.7	Serpentine	Wet	3.48	2.82	83.2	83.2	83.5
2	0	0.5	Serpentine	Wet	2.81	3.50	83.2	83.2	83.5
3	0	0	Serpentine	Wet	3.83	4.81	84.2	84.4	84.8
4	1.2	0	Serpentine	Wet	6.96	7.26	87.0	87.4	87.5

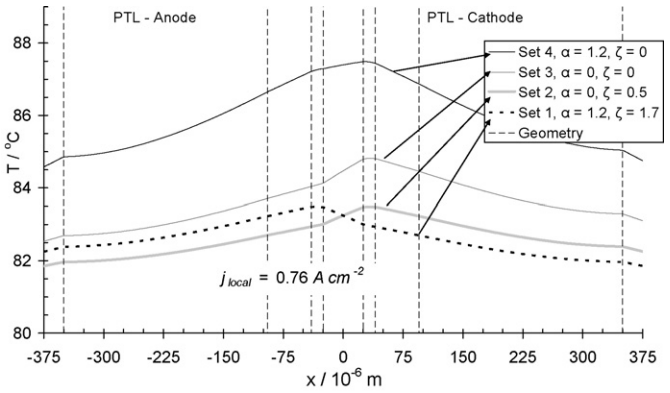

Fig. 3. Predicted temperature profiles under the centre of the gas channels. The model considers an average current density distribution of $j = 1\,A\,cm^{-2}$ and a local current density of $0.76\,A\,cm^{-2}$ imposed by a serpentine flow channel design. The control temperature in the polarisation plate was set to 80 °C.

the conditions considered in this model ($\lambda > 5$), the heat release is thus equal to the heat of vaporisation/condensation of water. In this model, this is controlled by two parameters: α and ζ. α corresponds to the number of water molecules per proton which absorbs into the membrane from the vapour phase, while ζ corresponds to the number of water molecules which desorbs to the vapour phase. Note that because the heat of desorption of water from the membrane to the gas phase is equivalent to the heat of vaporisation [17] we can speak interchangeably about desorption from the membrane to the gas phase and vaporisation of product water (and equivalently with regards to absorption to the membrane from the gas phase). For simplicity we mostly refer to adsorption and desorption meaning between the gas phase and the membrane. The maximum value that ζ can take is $\zeta_{max} = \alpha + 0.5$.

The gas channels are assumed to have stagnant gases which will slightly affect the local temperature distributions at the gas channel/PTL interface, but which is consistent with the assumption that all the heat generated in the system is removed by the cooling channels in the bi-polar plates. This is a reasonable assumption, as the amount of energy removed by the gas flows at these temperatures is small compared to the energy generated in the system.

All simulations were run until energy was conserved within at least 0.1% and the solutions were also shown to be mesh independent.

3. Model results

This paper considers and compares 2D thermal models of a fuel cell. The reference case for the comparison is what we regard as a reasonable best case scenario with respect to cooling the fuel cell. The reference case is suitably humidified, such that $\alpha = 1.2$, $\zeta = 1.7$, with a serpentine flow field (SFC 1 mm × 1 mm with 1 mm lands) with the maximum thermal conductivity in the porous transport layer (increased level due to residual water, anisotropic and non-homogenous thermal conductivity) when the polarisation plates are being operated at 80 °C and the average current density is $1\,A\,cm^{-2}$.

3.1. The nature of the system

The case described above is regarded as reference example for the results in this paper and is recognised as set 1 in Table 2. Figs. 3 and 4 depict the temperature profiles at the centre of the channel and at the centre of the land, respectively. Under the land,

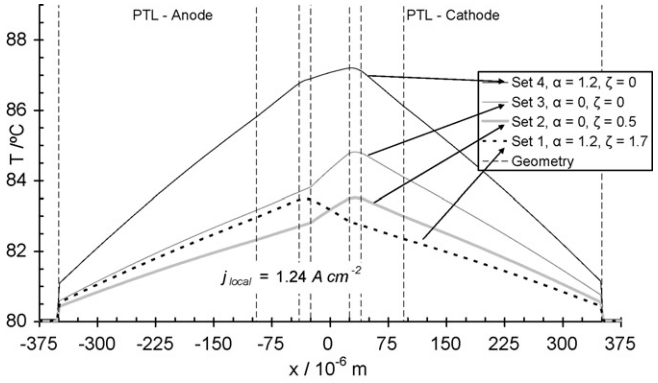

Fig. 4. Predicted temperature profiles under the centre of the ribs. The model considers an average current density distribution of $j = 1\,A\,cm^{-2}$ and a local current density of $1.24\,A\,cm^{-2}$ imposed by a serpentine flow channel design. The control temperature in the polarisation plate was set to 80 °C.

the maximum temperature occurs in the anode catalyst layer and is 3.5 °C above that of the bi-polar plate. The contact resistance between the bi-polar plate and the PTL results in a temperature jump of approximately 0.5 °C, and this jump is proportional to the heat flux passing through the interface which in this case is $3.48\,kW\,m^{-2}$ to the anode plate and $2.82\,kW\,m^{-2}$ to the cathode plate. The temperature profile is linear in the passive PTLs, and proportional to the heat flux, indicating that transport at this location is very nearly 1 dimensional. The contribution of the various heat sources is given in Fig. 5. The single largest contribution, representing −125% of the total heat leaving cell through the bi-polar plates, is the sink due to 1.7 moles of water per Coulomb of charge desorbing to the vapour phase at the cathode. The next largest term is the heat of absorption of 1.2 moles water per Coulomb of charge from the vapour phase at the anode representing approximately 88% of the heat conducted through the bi-polar plates. The heating due to activation polarisation in the cathode is nearly as significant, while the ohmic heating in the membrane is much smaller. It should be clear from this analysis that the state of water in the cell will be critical, both to the temperature distribution and to the amount of heat that must be removed by the cooling channels. This will be further discussed below.

The magnitude of the current distribution was set in order to try to make the membrane as isothermal as possible, and as such this case compares favourably to the results of a 1D simulation with the same conditions (set 0 in Table 2). These applied current density distributions are still in agreement with experimental and theoretical work [11–13]. It can be noted however that the 1D case represents the lowest maximum temperature possible. As more heat is generated under the channel, this heat will be transported through the PTL towards the land resulting in a maximum temperature under the gas channel. As such, a 2D model, considering multi-dimensional imposed effects, is essential to predict the maximum temperatures experienced in a cell.

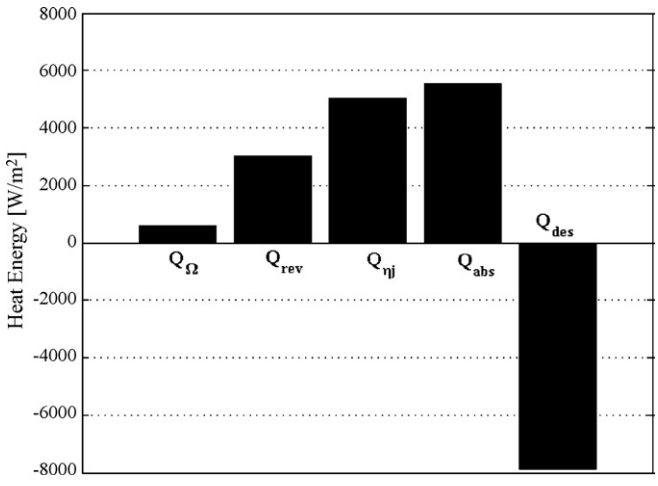

Fig. 5. Heat sources and heat sinks in a PEMFC, at 80 °C, $\alpha = 1.2$ and $\zeta = 1.7$.

3.2. The effect of water

The effect from absorption and desorption of water on the temperature distribution is shown in Figs. 3 and 4, under the channel and under the land, respectively. Additional data, including the heat conducted to the anode plate and the cathode plate is summarized in Table 2. The difference between set 1, set 2, set 3 and set 4 is the state of water in the PEMFC. For set 1, the reference case, 1.2 moles of water per Coulomb of charge absorbs into the membrane at the anode and then desorbs along with the product water at the cathode side. For set 2 we consider only the water product to evaporate at the cathode. Additional water can still be transported through the membrane in this case, but it is assumed to have come from the liquid phase such that no heat is liberated. For set 3 we consider all the water to be in its liquid state with no source terms due to absorption/desorption and for set 4 we assume that the dragged water reaches the anode from the vapour phase, but the cathode is saturated such that all the water leaves in the liquid state. We can think of these three cases as limiting cases with respect to water, and will find in reality, that different locations in an operating fuel cell may resemble each of them. We are therefore interested in how their thermal signature differs from one another so that we can see whether this issue is of great significance or not.

The temperature predictions for set 1 and set 2 are almost mirror images about the membrane centreline. Naturally, the corresponding heat flux conducted to the anode and cathode plate has also switched between the two cases. Consequently, the maximum temperature has moved from the anode in set 1 to the cathode in set 2. This behaviour can be explained by the fact that the heat of absorption is very significant and the impact of having α moles of water transported per proton is that significant energy is transported from the anode to the cathode. If, however, water is absorbed and desorbed from and to the liquid phase as in set 3, the maximum temperature in the fuel cell increases by more than one degree and occurs in the cathode catalyst. In addition, the total heat energy conducted to the bi-polar plates increases by approximately $2.3\,kW\,m^{-2}$. Set 4 represents an extreme case corresponding to running a fuel cell with 100% relative humidity in both the feed gases so that water can condense on the anode side but remains in the liquid phase at the cathode. In this case, the maximum temperature increases to 87.5 °C and the total heat conducted to the bi-polar plates increases to $14.2\,kW\,m^{-2}$, more than double the amount when all the water at the cathode is in the vapour phase. These cases serve to illustrate the significance of the state of water in the fuel cell on both the heat rejected to the cooling system and on the maximum temperature to which the fuel cell is subjected.

Another interesting thing we can learn from comparing possible water phase change effects is regarding the reversible heat production, $T\Delta Sj/nF$. For the model presented here, over 99% of the reaction entropy is solely related to the cathode process [15]. The distribution of the reversible heat between the anode and the cathode is a subject of some controversy [19], but from the above examples it is almost certain that redistribution will not change the maximum temperature. In reference to set 1 and set 2 it was shown that moving a more significant amount of heat energy from the anode to the cathode by the absorption and desorption of water was able to change the location of the maximum, but not its mag-

Table 3
Some temperatures and heat fluxes depending on thermal conductivities and water phase change conditions in a PEMFC operated with serpentine gas channel plates at 80 °C.

Set	α_{cond} (water proton^{-1})	ζ_{vap} (water proton^{-1})	PTL thermal conductivity conditions	Q'_{Anode} (kW m^{-2})	$Q'_{Cathode}$ (kW m^{-2})	T (25, 0) (°C (μm, mm))	T (25, 1) (°C (μm, mm))	T_{max} (°C
1	1.2	1.7	Wet	3.48	2.82	83.2	83.2	83.5
5	1.2	0	Dry	7.02	7.23	90.7	90.7	90.9
4	1.2	0	Wet	6.96	7.26	87.0	87.4	87.5
6	1.2	0	Increased cond.	6.72	7.45	82.0	83.1	83.2

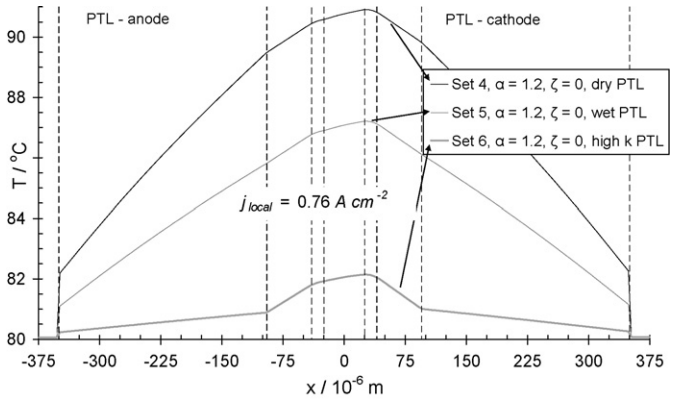

Fig. 6. Temperature profiles under the middle of the rib depending on thermal conductivities and water phase change conditions in a PEMFC operated with serpentine gas channels at 80 °C.

nitude. The reversible heat is exactly analogous to this, in that the sum of the anode and cathode reversible heats must be that of the overall reaction. Further, the magnitude of the reversible heat generation is noticeably smaller than the heat of absorption/desorption such that the details will pale in comparison.

The distribution of the reaction entropy among the two electrodes is set by nature and therefore impossible to control and the water phase change phenomena also presents some challenges to engineer. However, there are important parameters which can be applied to gain control of the temperature distribution in a fuel cell. One of them is related to modification of the thermal conductivity of fuel cell materials and another is the geometry of the fuel cell. It is to these effects that we now turn our attention.

3.3. Material thermal conductivities

The next subject to discuss is the material conducting the heat out of the fuel cell. In accordance with Fourier's law, the flux is equal to the thermal conductivity times the thermal gradient. Accordingly, if the heat flux remains the same, the temperature gradient will increase in proportion to the thermal conductivity. This is shown in Fig. 6 and in Table 3 which presents three cases of heat leaving the cell with a different through plane thermal conductivity for the PTL and different thermal contact resistance to the bi-polar plate. In all cases, the in-plane thermal conductivity corresponds to the base case, set 1. The lowest thermal conductivity and the highest contact resistance, set 5, correspond to the dry measurements of a SolviCore PTL undertaken in our lab [7]. As demonstrated [7], the in-plane thermal conductivity increases by 50% and the contact resistance decreases by 50% when residual water, is present in the PTL; this case is set 4. Finally, set 6 corresponds to a 10 fold increase of the through plane thermal conductivity and a 10 fold reduction of the contact resistance relative to set 5. This order of magnitude difference in the through plane thermal conductivity has recently been measured in different commercial materials using the technique reported in [7,22]. The effect of this difference is herein discussed based on experiments and a multi-dimensional model for the first time.

In comparing the temperature distributions, shown in Fig. 6, it is clear that these factors both have a significant effect on the maximum temperature. The maximum temperature ranges from 3.2 °C to almost 11 °C above the bi-polar plate temperature, with the contact resistance comprising between 0.5 and 2 °C of this difference. The total amount of heat generated in the system also decreases slightly as the temperature decreases since the reversible heat production is proportional to the temperature in the catalyst layer.

Table 4
Temperatures and heat fluxes in A PEMFC imposed by various gas flow channel designs (bi-polar plates operated at 80 °C).

Set	Flow channel design	PTL thermal conductivity conditions	Q'_{Anode} (kW m^{-2})	$Q'_{Cathode}$ (kW m^{-2})	$T(25, 0)$ (°C (μm, mm))	$T(25, 1)$ (°C (μm, mm))	T_{max} (°C)
1	Serpentine	Wet	3.48	2.82	83.2	83.2	83.5
7	Parallel/O_2	Wet	3.46	2.84	82.6	84.2	84.4
8	Parallel/air	Wet	3.58	3.01	82.1	85.3	85.7
9	Wide P. and air	Wet	3.52	3.10	81.4	90.2	90.6

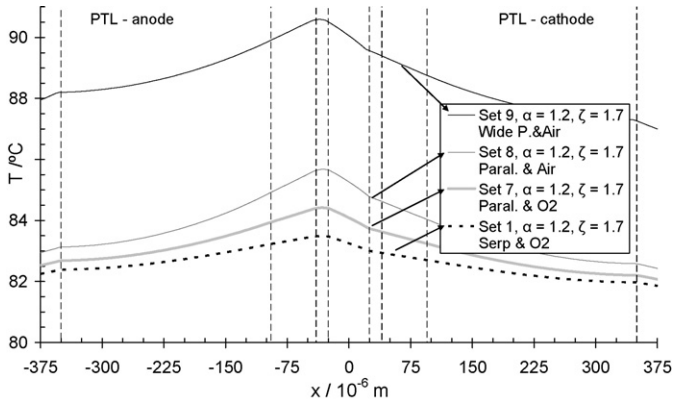

Fig. 7. Temperature profiles under the middle of the gas channels given for various current distribution imposed by gas flow channel design. The control temperature in the polarisation plate was set to 80 °C.

It is important to note, that these examples were carried out with fixed conditions for the phase of water in the system, and that the resulting temperature distributions are geometrically similar. It is reasonable to expect that the magnitude of the changes would be similar irrespective of the state of water. It is clear that care should be taken in designing PTL materials not just with respect to water transport, but also with regards to thermal conductivity.

3.4. Flow field design

The thermal conductivity is not the only parameter which can be tailored to influence the temperature distribution. The flow channel design can have a significant impact on the current distribution which controls where the heat is introduced into the system and consequently the temperature profile. Here we have accounted for this current distribution heating effect by imposing a current distribution which is consistent with more detailed observations of the impact of flow field on current density distribution [11–13], as discussed above. Notwithstanding the approximations inherent in this approach we shall discuss the results in terms of the physical interpretation. This section compares the temperature distributions which arise from having a maximum current under the land (serpentine flow field) to the case of having a maximum under the channel (parallel flow field). It also explores the effect of increasing the amplitude of the current distribution as in the normal case of using air instead of oxygen for the cathode feed. Finally the effect of increasing the channel and land dimensions is explored. In each case, all parameters are the same as in set 1 except for the current distribution and in the case of set 8, the channel width. The numerical results of this investigation are summarized in Table 4, while corresponding temperature profiles at the channel centreline are presented in Fig. 7.

On comparing set 1 and set 7, it can be seen that a current distribution consistent with a parallel flow field results in a maximum temperature which is about 1 °C higher than in the case of a serpentine flow field. This maximum occurs under the channel, since more heat is produced where the current is highest and all of this heat must be transported through the PTL to the bi-polar plate. So far, the assumed current distribution is quite modest, but when air is used as a feed, the amplitude can be much larger [11–13]. This is explored with set 8, with an increased amplitude for the current distribution and the result is an additional temperature increase of 1.5 °C. Finally, if the dimensions of the land and channel are doubled to 2 mm, as in set 9 the maximum temperature increases by an additional 5 °C as the length of the path from the region of heat generation to the bi-polar plate increases. This case represents a maximum temperature which is more than 10 °C

Table 5
Heat sources predicted in a fuel cell. Operating conditions are given in Tables 2–4.

Set	Q'_{rev} (kW m^{-2}) 2.98 at T = 80 °C	$Q'_{\eta j}$ (kW m^{-2}) 5.0 for η = 0.5 V	Q_{water} (kW m^{-2})	$Q'_{\Omega j}$ (kW m^{-2}) 0.57 for j = 1.0 A cm^{-2}	Q'_{tot} (kW m^{-2})	T_{max} (°C)
1	3.01	5.02	−2.32	0.59	6.30	83.5
4	3.05	5.02	5.56	0.59	14.22	87.5
5	3.08	5.02	5.56	0.59	14.25	90.9
8	3.02	5.13	−2.32	0.76	6.59	85.7
10[a] (4, 5 and 8)	3.10	5.13	5.56	0.76	14.55	95.3

[a] ζ = 1.2, α = 0, parallel flow channels and air, dry PTL.

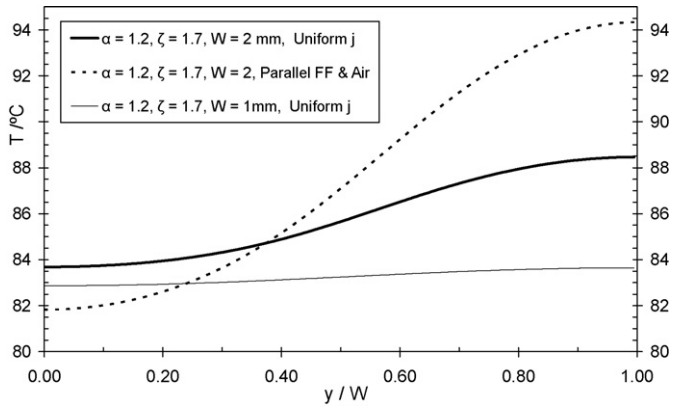

Fig. 8. Possible temperature profiles in the middle of the membrane along direction crossing the gas channels for polarisation plates held at 80 °C. This corresponds to the centre line in Fig. 1.

above the polarisation plate temperature and is the largest single effect shown. As such it warrants some further justification and exploration.

Fig. 8 shows the temperature distribution along the centre of the membrane for this case with a simulation imposing a uniform current density both for a 2 mm channel width and a 1 mm channel width. In the cases of uniform current density, the temperature profile is less extreme since proportionally more heat is generated under the land, but even with a uniform current density, the maximum temperature at the channel centreline increases by almost 5 °C as the channel and land width increase from 1 to 2 mm. This is explained by the fact that significantly more heat must travel laterally through the thin and relatively low conductivity PTL in order to reach the land. This example clearly shows that irrespective of the flow channel, or of the details of the current distribution, the effect of changing the channel dimension is very significant for the temperature distribution in the fuel cell. Smaller dimensions result in much more uniform temperatures, while larger dimensions can result in rather dramatic increases. As a comment to this observation, neutron imaging of water has revealed that water is less likely to form big droplets and further plug the gas channels when the channels are wide and parallel [20]. Similar effects are also observed by others [21]. These observations favour the use of broad parallel gas channels in order to avoid local flooding and impaired gas feed control. The present model demonstrates that increasing the channel width, such as proposed by the neutron imaging observations, leads to large increases in the maximum temperature because the local current density and reaction heat is concentrated further away from the cooling polarisation plate. Further, this increase in local temperature will also result in a locally increased water vapour saturation pressure and more water in the vapour phase. This effect could help explain the neutron imaging observations.

3.5. Lost work in the PEMFC fuel cell

Eq. (1) states that the total energy converted in a fuel cell is equal to the enthalpy of the reaction multiplied by the current. One component of this energy is the reversible heat, Q'_{rev}, which is given by, due to the temperature entropy product, i.e. $T\Delta S$. This heat is negative for the fuel cell reaction and thus increased temperature results in a decreased ability to extract work. Other fuel cells have a positive reaction entropy, such as the coal fuel cell, and the opposite behaviour is the case [23]. A contribution to the lost work is due to the activation overpotential, $Q'_{\eta j}$, and additionally the ohmic heat production, Q'_{Ω}. In Table 5 we predict the total

heat production contributions from the three mentioned terms depending on various situations. Model set 10 is a combination of set 4, set 5 and set 8. Considering parallel gas flow channels operated with maximally humidified gases and completely dry PTLs, so that we obtain an even higher maximum temperature in the fuel cell.

Because the reversible heat production depends on the local reaction temperature, we give its values both as a result from the local temperature and at the cell control temperature, 80 °C. The reversible heat production in Table 5 compared to the reversible heat at 80 °C, one can see that increased temperature in the cell increases the reversible lost work by up to 4%.

Next, Eq. (1) shows the heat production due to activation over potential. This term, $Q'_{\eta j}$, is not strongly dependent on whether the current density is imposed by a serpentine or a parallel gas flow pattern, but on the amplitude of the current density distribution. Quantitatively, running a fuel cell with air and a parallel gas flow pattern, the work lost by the over potential may increase by up to 2.5%. This value would in reality be strongly dependant on the actual fuel cell performance however, and would require a fully coupled electrochemical model to explore in more detail.

In consideration of the Ohmic heating in the membrane at 10 waters per sulphonic group, 8.7 S m^{-1}, with a 50 μm thick membrane and a current density of 1 A cm^{-2} the lowest possible ohmic heat production, Q'_{Ω}, is 0.57 kW m^2. Even though this gives the smallest contribution to the heat production in the fuel cell, according to Eq. (1) and Table 5, this term is still the most sensitive when considering current density distributions. This is simply because the ohmic heat production is proportional to the squared current density. Running the fuel cell with air and parallel gas flow channels we predict the lost work due to ohmic heating to be increased by 33%.

Thus comparing the work lost as heat in set 10 compared to the isothermal fuel cell at 80 °C with evenly distributed current density, the available work has in total decreased by 5%. We present here a simplification of other work studying the lost work in greater detail. The fact that the lost work is lowered by evenly distributed gradient is a known phenomenon [24]. The methodology regarding lost work is often referred to as entropy production. It should be expected that as even a distribution of entropy production will result in the least lost work as possible. In this case, this will correspond directly to as uniform a current as possible.

3.6. Stack considerations

It has thus far been shown that a single cell having a uniform temperature at the edge of the polarisation plates will experience significant temperature gradients. This will be notably worse in a stack. The equations solved here are linear which means that if the boundary condition temperatures are increased, the solution will increase correspondingly. This fact has significance with regards to the placement of cooling channels in a fuel cell stack, or indeed in making short stacks without cooling channels. If two adjacent cells are placed in contact without a cooling channel between them, it can be expected that to a very good approximation the effects shown here will be doubled as the increased temperature due to the first cell becoming the boundary condition to the next cell.

Thus far, we have considered only temperature gradients which arise due to heat generation due to electrical and electrochemical effects inside the fuel cell. In the case of a stack however, cooling is often effected by passing cooling water through the cooling channels, and this is also a driver for temperature gradients in cells and stacks. If we consider an automotive type stack of 75 kW it will be impossible to control the polarisation plates at uniform temperature as has been assumed thus far. The heat production in the stack can be as much as 1.5 times the electric power such that 113 kW of thermal energy would have to be removed by the coolant flow. The required flow rate to ensure that the temperature rise of the cooling water is kept below 10 °C would be approximately 2.5 l s^{-1}. Of course this flow rate must be minimized to ensure that the parasitic losses are minimized. The net result though is that it is not unreasonable to expect that the cooling channels will impose a significant variation in the polarisation plate temperatures and depending on the inlet temperature of the coolant, this would almost certainly result in increased maximum temperatures within the cell.

4. Conclusions

A simplified thermal model of a PEM fuel cell has been developed and used to explore the possible temperature gradients in the through plane of an operating fuel cell at 1 A m^{-2}. It has been shown that under no conditions is the cell isothermal even when both end plates are held at a constant temperature. Important parameters are the PTL thermal conductivity, which is significantly affected by the presence of liquid water, state of water in the anode and the cathode (absorption and desorption from the membrane) and the gas flow field design, with a particular sensitivity to the channel width. All things considered, it is very likely that the catalyst temperature is between 4 and 13 K higher than the end plate temperature. This assumes however that the endplates are held at a constant temperature: if the cooling channels are included, the increase will almost certainly be higher, and can be expected to double if cooling channels are only present in every second cell.

From a simple consideration of the lost work in a fuel cell, it can be expected that as uniform a current density distribution as possible will result in the least lost work, or the highest efficiency. There is a strong need to obtain a better understanding of the state of water in a fuel cell, and the location of any phase changes within the system, as this can have quite a large effect on the local temperature and hence on the maximum efficiency.

Acknowledgement

The Norwegian Research Council is acknowledged for financial support, grant number 164466/S30.

References

[1] P.J.S. Vie, S. Kjelstrup, Electrochim. Acta 49 (2004) 1069–1077.
[2] S. He, M.M. Mench, S. Tadigadapa, Sens. Actuators A 125 (2006) 170–177.
[3] G. Alberti, M. Casciola, L. Massinelli, B. Bauer, J. Membr. Sci. 185 (2001) 73–81.
[4] F. Bauer, S. Denneler, M. Willert-Porada, J. Polym. Sci. Part B: Polym. Phys. 43 (2005) 786–795.
[5] L.M. Onishi, J.M. Prausnitz, J. Newman, J. Phys. Chem. B 111 (2007) 10166–10173.
[6] Y. Zhai, H. Zhang, J. Hu, B. Yi, J. Membr. Sci. 280 (2006) 148–155.
[7] O. Burheim, P.J.S. Vie, J.G. Pharoah, S. Kjelstrup, J. Power Sources 195 (2010) 249–256.
[8] J. Ramousse, S. Didierjean, O. Lottin, D. Maillet, Int. J. Therm. Sci. 47 (2008) 1–6.
[9] F Danes, J. Bardon, Revue Generale de Thermique 36 (1997) 302–311.
[10] I. Nitta, T. Hottinen, O. Himanen, M. Mikkola, J. Power Sources 171 (2007) 26–31.
[11] J.G. Pharoah, K. Karan, W. Sun, J. Power Sources 161 (2006) 214–224.
[12] D. Harvey, J.G. Pharoah, K. Karan, J. Power Sources 179 (2008) 209–219.
[13] Mathias Reum, Stefan A. Freunberger, Alexander Wokaun, Felix N. Büchi, J. Electrochem. Soc. 156 (2009) B301–B310.
[14] C.J. Bapat, S.T. Thynell, ASME J. Heat Transfer 129 (2007) 1109–1118.
[15] M.J. Lampinen, M. Fomino, J. Electrochem. Soc. 140 (1993) 3537–3546.
[16] T.E. Springer, T.A. Zawodsisnki Jr., S. Gottesfeld, J. Electrochem. Soc. 138 (1991) 2334–2342.
[17] P.J. Reucroft, D. Rivin, N.S. Schneider, Polymer 43 (2002) 5157–5161.
[18] K.D. Kreuer, Solid State Ion. 97 (1997) 1–15.
[19] J. Ramousse, O. Lottin, S. Didierjean, D. Maillet, J. Power Sources 192 (2009) 435–441.
[20] A. Turhan, K. Heller, J.S. Brenizer, M.M. Mench, J. Power Sources 180 (2008) 773–783.

[21] P. Boilat, D. Kramer, B.C. Seyfang, G. Frey, E. Lehmann, G.G. Scherer, A. Wokaun, Y. Ichikawa, Y. Tasaki, K. Shinora, Electrochem. Commun. 10 (2008) 546–550.
[22] O. Burheim, H. Lampert, P.J.S. Vie, J. Pharoah, S. Kjelstrup, Through-Plane Thermal Conductivity of PEMFC Porous Transport Layers (PTLs), J. Fuel Cell Sci. and Techn.
[23] K. Hemmes, G.P.J. Dijkema, H.J. van derKooi, Russ. J. Elecrochem. 40 (2004) 1284–1288.
[24] E. Johannessen, S. Kjelstrup, Chem. Eng. Sci. 60 (2005) 3347–3361.